VAGUE D'ÉTRAVE ET FONCTION DE GREEN

SHIP BOW WAVE AND GREEN FUNCTION METHOD

FRANCIS NOBLESSE*, GERARD DELHOMMEAU, CHI YANG*****

* NSWCCD, Bethesda MD, USA; francis.noblesse@navy.mil
** ECN-CNRS, Nantes, France; gerard.delhommeau@ec-nantes.fr
*** George Mason University, Fairfax VA, USA; cyang@gmu.edu

Résumé

Ce papier — écrit à l'occasion du départ à la retraite du second auteur — résume les principaux résultats des travaux communs récents des auteurs concernant le développement de relations analytiques simples et d'outils pratiques de calcul pour évaluer l'écoulement autour d'une carène animée d'une vitesse constante en eau calme. Le papier traite de deux sujets principaux : (a) l'établissement d'expressions analytiques permettant de prédire la vague d'étrave qui est un aspect important de l'écoulement autour d'une carène et (b) une méthode très simplifiée de calcul de l'écoulement en utilisant une fonction de Green, aussi appelée méthode des singularités ou des éléments frontières. Les résultats de ces deux études peuvent être utilisés pour définir rapidement et optimiser la forme des carènes au niveau de l'avant-projet, y compris l'étude de concept et le dessin préliminaire.

Summary [1]

This paper — written to mark the retirement of the second author from the École Centrale of Nantes — summarizes the main results of the authors' recent joint work related to the development of simple analytical relations and practical computational tools for evaluating the flow about a ship hull steadily advancing in calm water. This paper summarizes our work on two main topics : (a) analytical relations for predicting ship bow waves, an important particular aspect of the flow about a ship hull, and (b) a highly-simplified flow-calculation method based on the Green function method, also widely known as the boundary element or panel method. The analytical relations for ship bow waves and the flow-calculation method are well suited for routine applications at early ship design stages, including concept and preliminary design, and hull-form optimization.

1. The support of the Office of Naval Research (Technical Monitor : Ms. Kelly Cooper) and the ILIR Program at NSWCCD (Technical Monitor : Dr. John Barkyoumb) is gratefully acknowledged.

INTRODUCTION

The first two authors' close cooperation on joint research work began as a result of the first author's two-month visits at the École Centrale of Nantes in 2004 and at the University of Poitiers in 2005. Specifically, our cooperation dates from the spring of 2005 when Prof. Michel Guilbaud of the University of Poitiers and the authors began working together on the development of a simple approximate theory of overturning ship bow waves. The results of the authors' joint research work are reported in references [1-8] and in a number of papers presented at various conferences. As indicated in [1-8], the authors have also benefited from their cooperation with several researchers on both sides of the Atlantic ocean ; specifically Prof. Michel Guilbaud and Prof. Laurent David of the University of Poitiers, Dr. Patrick Queutey of the École Centrale of Nantes, and Dr. Hyun Yul Kim and Mr. Fuxin Huang of the George Mason University. Our joint research work on two topics related to the 3D flow about the hull of a ship that advances, at constant speed along a straight path, in calm water of effectively infinite depth and lateral extent is summarized here. Applications to ship hull-form optimization are not considered here.

The first research topic seeks to obtain simple analytical relations — readily suited for applications to ship design, notably concept and preliminary design — for predicting the bow wave generated by a steadily advancing ship hull. This work has been pursued for two main reasons : a practical motivation and a simple theoretical consideration. The practical motivation is that a ship bow wave is arguably the most visible, complex and important feature of the flow due to a steadily advancing ship, and is of interest for design. The theoretical consideration is that the flow due to a ship hull (steadily advancing in calm water) consists of a wave component that propagates downstream (and is then located behind the ship stem), and a local-flow component that is significantly smaller than the wave component (except at very low Froude numbers). As a result, a ship bow wave is not appreciably affected by the length of the ship or by the shape of the ship stern and midbody, and in fact is mostly determined by the size and shape of the ship bow. The bow wave generated by a ship hull can therefore be determined, a priori, for several classes of ship bows, which can be defined in terms of a limited number of parameters. Specifically, a four-parameter family of fine nonbulbous bows and a more general seven-parameter family of bulbous bows are sufficient to approximately represent most ship bows.

The second topic of our research is the development of a simple practical computational method, based on the classical Green function method (also known as the Boundary Element Method and the panel method), for evaluating 3D potential flow about a steadily advancing ship hull. This work is motivated by the practical need for a computational method that is suited for routine applications to hydrodynamic design and hull-form optimization. Another motivation is the authors' quest to finally find a fully satisfactory way, and hence to not die complete idiots, for applying the Green function method to compute 3D flow about a ship ; a notoriously 'hard' problem that has been a longstanding source of frustration to many hydrodynamicists, the authors included.

Our work on ship bow waves has led to three main results : simple analytical relations that determine (a) the bow wave profile and (b) the boundary between two basic flow regimes (unsteady and 'steady' overturning bow waves) for a broad class of fine ship bows, and (c) a simple theory that approximately predicts the size, the shape, and the thickness of an overturning ship bow wave and the main geometrical characteristics of the related wavebreaking wake. The work on the development of a practical Green function method has led to two main results : (a) remarkably simple Green functions — for the general case of flow about an arbirary ship hull, and for two special cases that correspond to ACV (Air Cushion Vehicles) and planing hulls (associated with the flow due to a free-surface pressure patch) and thin ships (thin-ship theory) — and (b) a highly-simplified flow representation, and related calculation method, that only involves continuous ordinary functions (algebraic, exponential and trigonometric functions) of real arguments. These main results are now summarized.

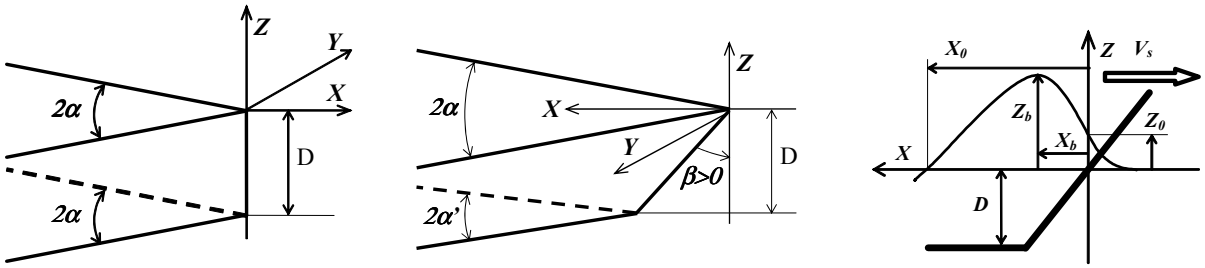

Figure 1 – Left side : Two-parameter family of wedge-shaped ship bows defined by the draft D and the waterline entrance angle 2α. Center : Four-parameter (draft D, rake angle β, and entrance angles 2α and $2\alpha'$ of top and draft waterlines) family of ship bows with rake and flare. Right side : Ship draft D and speed V_s, rise of water Z_0 at the ship stem, bow wave height Z_b, distance X_b between the ship stem and the bow wave crest, and distance X_0 between the ship stem and the crossing of the bow wave with the mean free-surface plane $Z = 0$.

I – ANALYTICAL SHIP BOW WAVES

I – 1 Analytical bow wave profiles for fine nonbulbous ship bows

Two simple classes of nonbulbous ship bows — the two-parameter family of wedge-shaped bows and the more general four-parameter family of bows with rake and flare depicted on the left side and in the center of Fig.1 — have been considered. The family of wedge-shaped bows is a special case, that corresponds to $\beta = 0$ and $\alpha' = \alpha$, of the family of bows with rake and flare. Both positive ($0 < \beta$) and negative ($\beta < 0$) rake angles have been considered.

As illustrated on the right side of Fig.1, a ship bow wave profile is largely determined in terms of four main 'primary' variables : the wave height Z_b, the distance X_b between the ship stem and the wave crest, the rise of water Z_0 at the ship stem, and the 'length' X_0 of the wave (location, measured from the ship stem, of the intersection of the bow wave profile with the mean free-surface plane $Z = 0$). These four primary variables have been considered for the simplest (two-parameter) class of wedge-shaped bows and, subsequently, for the more general (four-parameter) family of bows with rake and flare. Specifically, wedge-shaped bows are considered in [9] where simple analytical relations for Z_b and X_b are given, in [1] where a simple analytical expression for Z_0 is given, and in [2] where the relations for Z_b, X_b and Z_0 are summarized and considered further. These relations for wedge-shaped bows are extended to the more general family of ship bows with rake and flare in [4] and finally in [6], where X_0 and the wave profile are also considered.

Thus, the four primary variables Z_b, X_b, Z_0, X_0 can be estimated using simple analytical relations. E.g., for a wedge-shaped bow with draft D and waterline entrance angle 2α, the wave height Z_b is given by

$$\frac{Z_b\, g}{V_s^2} \approx \frac{2.2}{1+F}\,\frac{\tan\alpha}{\cos\alpha} \quad \text{with} \quad F \equiv \frac{V_s}{\sqrt{gD}}\,. \tag{1}$$

Here, g and V_s stand for the acceleration of gravity and the ship speed, respectively. The relation (1) for the wave height Z_b and the corresponding relation for the location X_b of the wave crest are obtained in [9] for wedge-shaped bows using both elementary theoretical considerations (notably dimensional analysis and basic asymptotic considerations) and experimental measurements. The expression for Z_0 given in [1] is based on thin-ship theory. This theory is also used in [4] and [6] to extend the relations for Z_b, X_b, Z_0 given in [9,1,2] for wedge-shaped bows to a (four-parameter) family of bows with rake and flare, and to consider X_0 and bow wave profiles for this more general family of bows.

Theoretical predictions given by the relation (1) for Z_b and the corresponding relations for X_b and Z_0 are compared with experimental measurements in [9,1,2] and with numerical predictions given by thin-ship theory and CFD in [4,6]. E.g., Fig.2 shows a comparison of the wave height

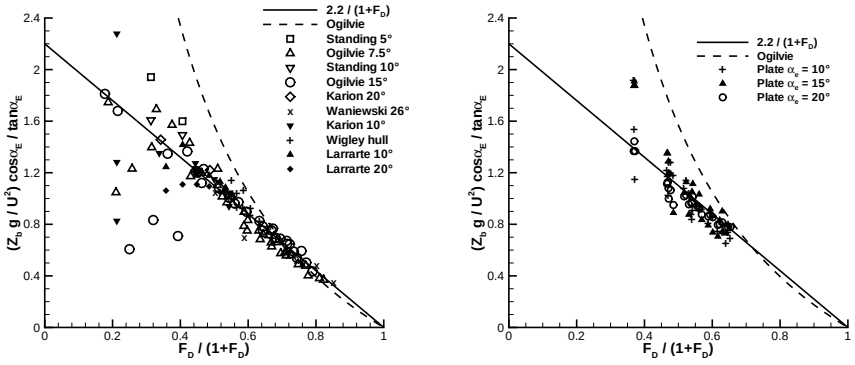

Figure 2 – Normalized bow wave height $(Z_b\, g/V_s^2)\cos\alpha\,/\,\tan\alpha$ for ten hull forms (left), and a rectangular flat plate towed at several speeds V_s, yaw (incidence) angles α and heel angles γ (right). The straight solid line is the approximation (1) and the dashed curve corresponds to Ogilvie's high-Froude-number approximation.

Z_b predicted by the simple relation (1) and experimental measurements for ten wedge-shaped bows and a rectangular flat plate towed at various speeds V_s and yaw angles α.

The relations for Z_b, X_b, Z_0, X_0 given in [6] provide insight into the influence of basic design parameters like the Froude number F (ship speed V_s and draft D) and parameters associated with the bow shape (rake angle β, waterline entrance angles α and α', and related flare parameter) for a broad class of ship bows. E.g., the relations yield

$$Z_0/D = O(1) \qquad Z_b/D = O(F) \qquad X_b/D = O(F) \qquad X_0/D = O(F^2) \qquad \text{as } F \to \infty\,.$$

Thus, the height Z_b of a ship bow wave and the distance X_b between the ship stem and the bow wave crest increase in proportion to the ship speed V_s as $V_s \to \infty$; however, the rise of water Z_0 at a ship stem tends to a constant value as $V_s \to \infty$, and the length X_0 of the bow wave increases as V_s^2 in the high-speed limit.

The bow wave profile is determined from the four primary variables Z_b, X_b, Z_0, X_0. Specifically, the front and back of the bow wave profile are approximated by two parabolic arcs, as in Fig.3. This figure also depicts wave profiles given by thin-ship theory and two Euler-flow CFD computations, for the ship bow shown in Fig.1 with $\beta = 30°$ and $\alpha' = \alpha = 15°$, at four draft-based Froude numbers $F = 0.67$, 1, 1.5, 2.33. The Euler wave profiles in Fig.3 were obtained using the flow solvers ISIS-CFD and FEFLO developed at ECN-CNRS and at GMU, respectively [10-12]. A ship hull with fore and aft symmetry, and length/draft ratio equal to 40, was used for the Euler-flow calculations. Fig.3 shows that the analytical bow wave profiles are comparable to the Euler (CFD) wave profiles, and that the Euler profiles are appreciably closer to the analytical bow wave profiles than to the wave profiles given by thin-ship theory.

Thus, the simple analytical relations for the four primary variables Z_b, X_b, Z_0, X_0 and the related parabolic wave profile readily provide estimates of ship bow waves for a broad class of nonbulbous ship bows. These estimates, comparable to CFD predictions, can be used immediately — without hydrodynamic calculations, and at a computational cost that is null — for design, notably at early design stages when the precise hull geometry may not yet be known, and within a multi-objective optimization scheme. The relations and the systematic parametric studies reported in [4,6] also provide useful insight.

I – 2 Boundary between unsteady and overturning bow wave regimes

The bow wave generated by a ship (that advances at constant speed along a straight path in calm water) can be unsteady, or can consist of an overturning detached thin sheet of water that is mostly steady until it hits the undisturbed free surface. An example of these two basic flow regimes — the 'unsteady bow wave regime' and the 'overturning bow wave regime' — is shown in Fig.4. The boundary between these flow regimes is determined in [2] from the relation

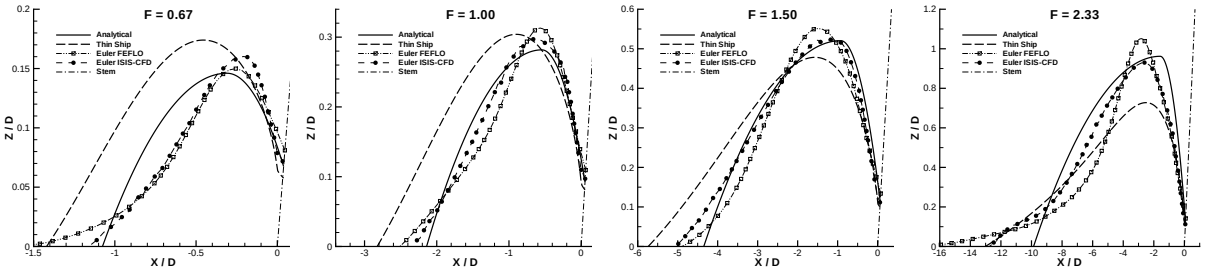

Figure 3 – Analytical (parabolic) wave profiles and wave profiles obtained from thin-ship theory and two CFD flow solvers (ISIS-CFD and FEFLO), used in Euler-flow mode, for the ship bow shown in Fig.1 with $\beta = 30^\circ$ and $\alpha' = \alpha = 15^\circ$, at four draft-based Froude numbers $F = 0.67$, 1 , 1.5 and 2.33 .

(1) for the bow wave height and the upper bound $Z_b\, g/V_s^2 \leq 1/2$ for steady free-surface flows, which readily yields

$$4.4 \tan\alpha / \cos\alpha \leq 1 + F . \tag{2}$$

This relation for wedge-shaped bows is readily extended to the more general class of ship bows with rake and flare [3,6] .

The upper bound $Z_b\, g/V_s^2 \leq 1/2$ for steady free-surface flows also shows that the height of an unsteady ship bow wave is given by $Z_b \approx V_s^2/(2\, g)$. Thus, the height of an unsteady ship bow wave only depends on the ship speed V_s , and is independent of the ship draft D or the bow shape. Experimental validation of this simple theoretical result is reported in [2] .

The relation (2) shows that a ship with a sufficiently fine waterline, specifically with entrance angle 2α smaller than approximately 25°, may generate a steady overturning bow wave at any speed. However, a ship with a fuller waterline ($25^\circ < 2\alpha$) can only generate a steady bow wave if the ship speed is higher than a critical speed that is defined in terms of the bow shape by the simple analytical relation (2). Experimental validation of the theoretical boundary (2) separating the unsteady and overturning bow wave regimes is given in [3,2] . Specifically, qualitative observations (photographs and videos) and quantitative measurements of fluctuations of the bow wave profile have been performed and are reported in [3,2] for the bow wave generated by a rectangular flate plate towed at various speeds V_s , yaw (incidence) angles α and heel angles γ . These flow observations and measurements show that the remarkably simple relation (2) appears to correctly predict if a ship bow wave can be expected to be unsteady or overturning.

I – 3 A simple approximate theory of overturning ship bow waves

As already noted, the bow wave generated by a ship can be unsteady or can consist of an overturning detached thin sheet of water that is mostly steady until it hits the undisturbed free surface. The 'steady' overturning ship bow wave regime, which mostly occurs for ships with fine bows, is considered in [7] .

Experimental investigations of ship bow waves, notably overturning bow waves, have been reported in the literature ; a partial list of references to these experimental studies may be found in [7] . Overturning ship bow waves cannot be predicted using traditional theoretical methods, notably thin-ship theory and potential-flow panel methods, for computing flow about a ship hull. However, divergent overturning ship bow waves can be predicted and evaluated using the 2d+t theory and some numerical (CFD) methods. A partial list of references to these numerical studies is also given in [7] .

Recent 'advanced' CFD methods can be used to compute overturning detached ship bow waves, as is well advertised in this conference. However, such numerical calculations require a fine discretization to resolve the detached wave, and are ill suited for routine applications to design, notably at early stages when a large number of alternative designs often need to be considered. These numerical methods likewise are ill suited for systematic parametric studies

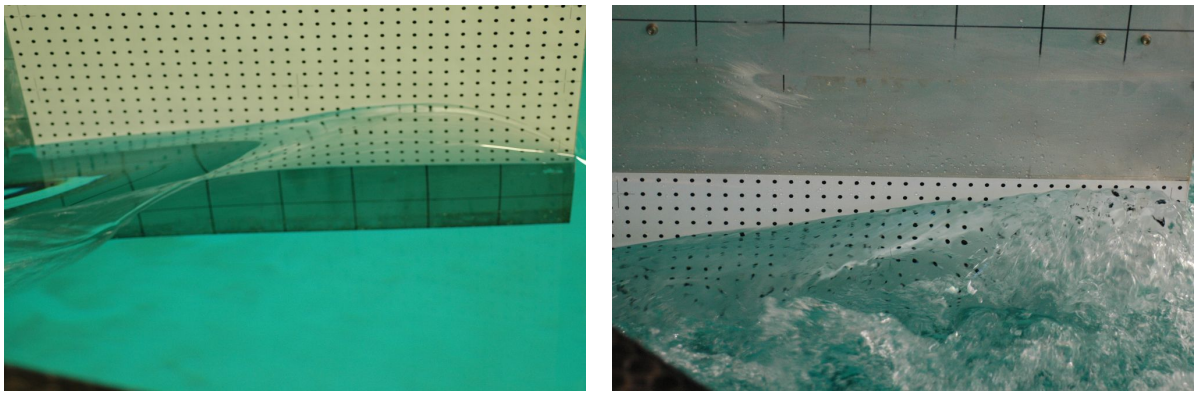

Figure 4 – Examples of steady overturning (left side) and unsteady (right side) bow wave due to a vertical rectangular flat plate. The flat plate, immersed at a draft $D = 0.2$ m, is towed at a yaw (incidence) angle $\alpha = 15°$ (left) or 45° (right) and a speed $V_s = 2.25$ (left) or 2 (right) m s^{-1}. The corresponding draft-based Froude numbers are $F \approx 1.61$ (left) and 1.43 (right).

to determine the influence of a ship's speed and draft, and of the shape of a ship bow, on the overturning bow wave and the related wavebreaking wake.

Indeed, neither advanced numerical methods nor experimental investigations are well suited for performing systematic parametric studies designed to yield 'cause-and-effect' relations that readily provide insight into the influence of a ship's speed and draft, and of main parameters that approximately define the bow shape — entrance angles at the top and bottom waterlines, rake angle, and flare — on the overturning bow wave, and the related wavebreaking wake, generated by a ship. Indeed, none of the previously listed experimental or numerical investigations present parametric studies from which 'cause-and-effect' relations can be obtained. The main practical objective of the simple approximate analytical theory expounded in [7] is to provide such 'cause-and-effect' relations, albeit approximate ones, that can be applied immediately — without hydrodynamic calculations, and at a computational cost that is essentially null — notably at early design stages when the bow shape is not yet fully determined.

The simple theory reported in [7] ignores effects of viscosity and surface tension. Although this basic approximation greatly simplifies the flow analysis, the inviscid-flow analysis of an overturning ship bow wave remains extremely complex, notably due to strong nonlinearities in the free-surface boundary condition. Additional approximations are then required, and are made in the simple theory expounded in [7] . However, this theory accounts for nonlinearities in the free-surface boundary condition.

The theory consists of four main steps. The initial step is the contact curve — commonly called bow wave profile — between the ship hull and the free surface. This step is considered in [6,4] for the broad class of fine ship bows depicted in the center of Fig1 . In the second step, previously considered in [13] , the flow velocity at the bow wave profile is determined — analytically in terms of the bow wave profile — from the exact (for an inviscid flow) boundary conditions at the ship hull surface and the free surface. The third step is an elementary Lagrangian analysis, based on Newton's equations, to determine the motion of water particles within the overturning detached bow wave and the wave's size, shape, and intersection with the mean free surface. The fourth step determines the thickness of the overturning detached ship bow wave by relating the volume of water that flows through an overturning bow wave to the water displaced by the advancing ship hull. These four steps fully determine the size, shape and thickness of an overturning detached bow wave and the related wavebreaking wake in terms of the ship speed, the bow geometry (draft and shape) and the bow wave profile. The theory is then particularly simple, and markedly different from alternative approaches.

A main recommendation of the theory is that it yields simple, albeit approximate, relations that provide insight into the influence of a ship's speed and draft, and of major parameters

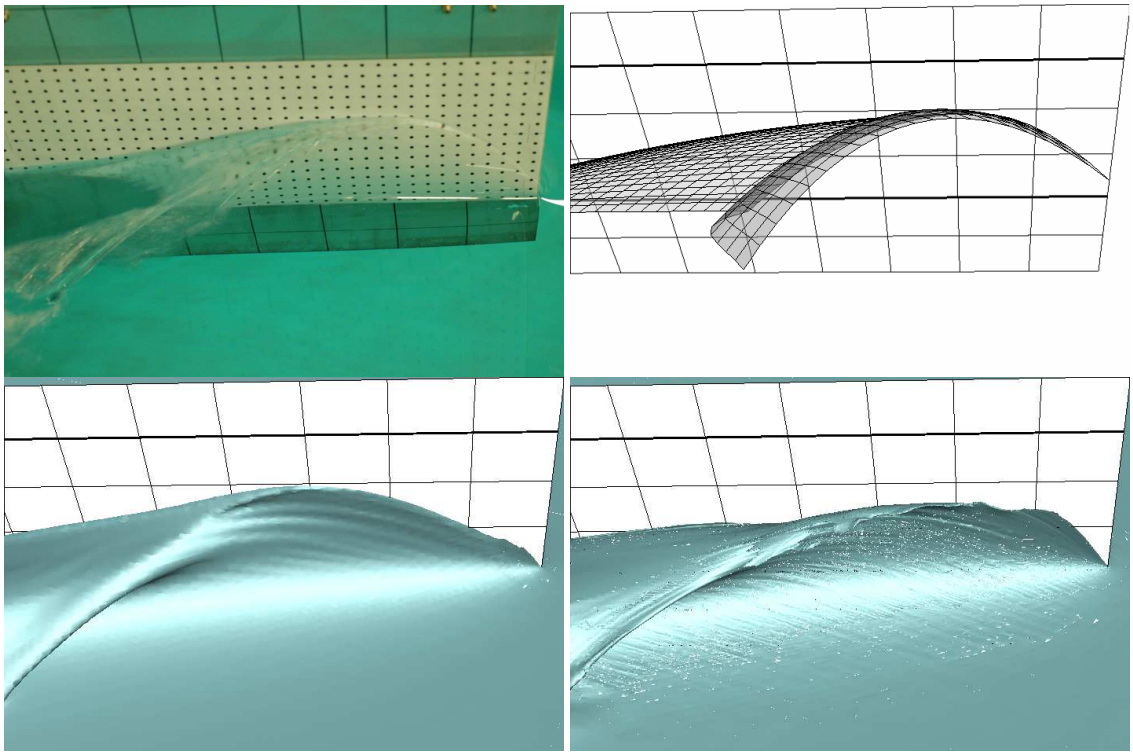

Figure 5 – Experimental observation (photograph on upper left corner), numerical solutions of Euler (lower left) or RANS (lower right) equations given by the CFD flow solver ISIS-CFD, and theoretical prediction (upper right) of bow wave generated by a rectangular flat plate, of draft $D = 0.2$ m and length 0.782 m , towed at a speed $V_s = 2.5$ m/s , a yaw angle $\alpha = 20°$, and a heel angle $\gamma = 15°$.

related to the bow shape (entrance angles at the top and bottom waterlines, rake angle, and flare) on the overturning bow wave, and the related bow wavebreaking wake. These analytical relations can be applied immediately — at a computational cost that is null for all practical purposes — for design, notably at early stages when the bow shape may not yet be known precisely. The relations can also be used to extend the capabilities of calculation methods like thin-ship theory or panel methods.

Fig.5 shows a comparison of theoretical predictions with experimental observations and numerical calculations. Specifically, numerical solutions — obtained using the CFD flow solver ISIS-CFD [10] — based on Euler or RANS equations are shown in the lower left or right corners, respectively, of Fig.5 for a rectangular flat plate towed at a speed $V_s = 2.5$ m/s, a yaw angle $\alpha = 20°$ and a heel angle $\gamma = 15°$. The 'theoretical bow wave' predicted by the simple approximate theory and the 'experimental bow wave' are shown in the upper right or left corners, respectively. The bow wave height predicted by the RANS numerical computations is appreciably smaller than the experimental wave height and the wave heights predicted by the Euler solution and the analytical theory, which all agree fairly well. The 'Euler wave crest' appears to be located further away from the leading edge of the plate (stem) than the experimental and theoretical wave crests, which are in fairly good agreement. In fact, the theoretical wave profile appears to better agree with the experimental profile than the Euler and RANS profiles. However, the overturning bow wave predicted by the theory is significantly shorter than the experimental bow wave and the 'numerical bow waves' (both Euler and RANS), which all appear to be in good agreement. The thickness of the overturning bow wave predicted by the theory for the case considered in Fig.5 is approximately 0.5cm, which is consistent with experimental observations (the circular dots on the plate shown in the upper left corner of Fig.5 are 0.5cm in diameter and spaced 2cm apart in the horizontal and vertical directions). Thus, the theory appears to yield

realistic predictions of the size, shape and thickness of overturning ship bow waves.

II – PRACTICAL GREEN FUNCTION METHOD

Alternative methods for evaluating steady free-surface flows about ships in deep water have been considered in the literature. These methods include semi-analytical theories based on various approximations (thin-ship, slender-ship, 2d+t theories), potential-flow panel (boundary integral equation) methods that rely on the use of a Green function (elementary Rankine source, or Havelock source that satisfies the radiation condition and the Kelvin-Michell linearized free-surface boundary condition), and computational fluid dynamics (CFD) methods that solve the Euler or RANS equations. These alternative calculation methods are reported in a huge body of literature, not reviewed here ; a partial list of references may be found in e.g. [2] .

Selection of a flow calculation method requires consideration of a tradeoff between competing requirements with respect to accuracy and practicality. Indeed, practical tools that are simple to use and highly efficient, but need not be highly accurate, are required to quickly evaluate the very large number of alternative designs that typically need to be considered for concept and preliminary design and for hydrodynamic optimization. However, detail design and design evaluation involve many fewer choices and require more accurate computational tools, for which efficiency and ease of use are less important. Thus, highly-efficient (in terms of user input time and CPU) and robust approximate methods are important for many practical applications, notably for early design stages (concept and preliminary design) and for hull-form optimization ; e.g., [21-25] .

A classical approximate method is the potential-flow panel method based on a Green function that satisfies the radiation condition and the Kelvin-Michell linearized boundary condition at the free surface. Two well-known major recommendations of this approach are (a) that the farfield boundary condition (including the radiation condition) is satisfied — automatically and exactly — via the Green function, and (b) that the flow in the *infinite 3D flow domain* outside a ship is formulated over the *finite 2D ship hull surface*.

II – 1 Highly-simplified Green functions

However, this remarkable simplification comes at the price of a relatively complicated Green function. This Green function can be expressed as the sum of three components : (a) a wave component defined by a single Fourier integral with continuous integrand, (b) the fundamental free-space Green function $1/r$ where r is the distance between the source point $\mathbf{x} \equiv (x\,,y\,,z)$ and the flow-field point $\widetilde{\mathbf{x}} \equiv (\widetilde{x}\,,\widetilde{y}\,,\widetilde{z})$ in the Green function $G \equiv G(\widetilde{\mathbf{x}},\mathbf{x})$, and (c) a local flow component that is given by a double Fourier integral with singular integrand. The singular double Fourier integral can be transformed into a single integral, with integrand expressed in terms of the exponential integral function $E_1(\zeta)$ with a complex argument ζ .

Three alternative single-integral representations of the local flow component and the corresponding Green function are given in [14] , including the well-known representation

$$4\pi G = H(x-\widetilde{x})\frac{4}{F^2}\,\Im\mathrm{m}\int_{-t_\infty}^{t_\infty} dt\,\Lambda\, e^{\,(1+t^2)\,(\widetilde{z}+z)/F^2 + i\sqrt{1+t^2}\,[\widetilde{x}-x+t\,(\widetilde{y}-y)]/F^2} - \frac{1}{r} + G^L. \qquad (3)$$

The coordinates of the source point $\mathbf{x}$ and of the flow-field point $\widetilde{\mathbf{x}}$ in the Green function $G(\widetilde{\mathbf{x}},\mathbf{x})$ are nondimensional in terms of a reference length L_{ref} , e.g. the ship length L_s or V_s^2/g where V_s stands for the ship speed and g is the acceleration of gravity. Thus, we have $\mathbf{x} \equiv (x\,,y\,,z) \equiv (X,Y,Z)/L_{ref}$ and $\widetilde{\mathbf{x}} \equiv (\widetilde{x}\,,\widetilde{y}\,,\widetilde{z}) \equiv (\widetilde{X},\widetilde{Y},\widetilde{Z})/L_{ref}$. The first term in the classical integral representation (3) of G is the wave component, where $H(\cdot)$ stands for the usual Heaviside unit-step function, $\Im\mathrm{m}$ means that the imaginary part is considered, $F \equiv V_s/\sqrt{g\,L_{ref}}$ is the Froude

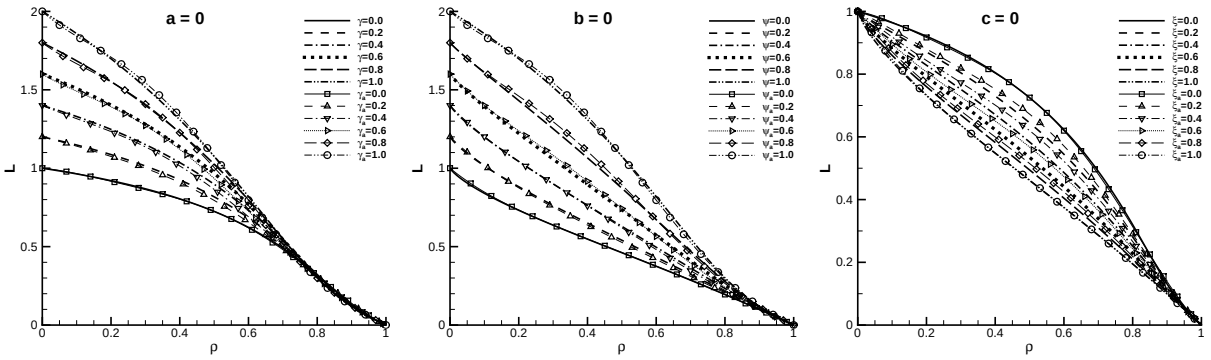

Figure 6 – Function L in expression (4) for the local flow component G^L in the Green function G for the three particular cases $a = 0$ (left), $b = 0$ (center) or $c = 0$ (right), i.e. for $\widetilde{x} - x = 0$, $\widetilde{y} - y = 0$ or $\widetilde{z} + z = 0$. The function L is evaluated using the (exact) integral representation (4) or the simple approximation (6).

number, and the function Λ filters irrelevant unrealistic short waves for $t_\infty < |t|$. The local flow component G^L in (3) is given by

$$G^L = \frac{1}{r_1} - \frac{2L}{F^2} \quad \text{with} \quad L \equiv 1 + \frac{c}{d+a} - \frac{1}{\pi}\int_{-1}^{1} dt\, \Im\mathrm{m}\,[\, e^{\zeta} E_1(\zeta) + \ln(\zeta)\,]\,. \tag{4}$$

Here, $\zeta \equiv (b\,t - c\sqrt{1-t^2} + i\,a)\sqrt{1-t^2}$ with $a \equiv |\,\widetilde{x} - x\,|/F^2$, $b \equiv |\,\widetilde{y} - y\,|/F^2$, $c \equiv -(\widetilde{z}+z)/F^2$ and $d \equiv \sqrt{a^2+b^2+c^2} \equiv r_1/F^2$. The coordinates a, b, c and the related distance d are ≥ 0 and nondimensional with respect to the reference length $L_{ref} = V_s^2/g$. In (3) and (4), r and r_1 are defined as

$$r \equiv \sqrt{(\widetilde{x}-x)^2 + (\widetilde{y}-y)^2 + (\widetilde{z}-z)^2}\,, \qquad r_1 \equiv \sqrt{(\widetilde{x}-x)^2 + (\widetilde{y}-y)^2 + (\widetilde{z}+z)^2}\,. \tag{5}$$

Clearly, r and r_1 represent the (nondimensional) distances between the flow-field point $\widetilde{\mathbf{x}} \equiv (\widetilde{x}\,, \widetilde{y}\,, \widetilde{z}\,)$ and the source point $\mathbf{x} \equiv (x\,, y\,, z)$ or its mirror image $\mathbf{x}_1 \equiv (x\,, y\,, -z)$ with respect to the mean free-surface plane $z = 0$.

Nearfield and farfield asymptotic approximations to the local flow component G^L are given in [15-18]. Approximations based on polynomial expansions [18] or table interpolation [19,20] in complementary contiguous regions of the flow domain have also been given. Considerably simpler alternative approximations — that are *fully-analytical* and valid within the *entire flow region* — to the local flow component in the Green function $G(\widetilde{\mathbf{x}}, \mathbf{x})$ have been obtained by the authors for two special cases that correspond to flows due to thin ships [4] and air-cushion-vehicles or planing boats [5], for which we have $\widetilde{y} - y = 0$ or $\widetilde{z} + z = 0$, and for the general case when the source point $\mathbf{x}$ and the flow-field point $\widetilde{\mathbf{x}}$ in the Green function $G(\widetilde{\mathbf{x}}, \mathbf{x})$ are arbitrary [8].

Specifically, the local flow component G^L in the representation (3) of the Green function G is given by the analytical approximation

$$G^L \approx \frac{1}{r_1} - \frac{2}{F^2 + r_1} - \frac{2\,F^2\,\psi}{(F^2+r_1)^2} - \frac{0.4\,F^2\,r_1}{(F^2+r_1)^5}\,[\,(A + B\gamma)(1-\xi) - F^2 C\,\xi\,]\,. \tag{6}$$

Here, r_1 is given by (5), and A, B, C and ξ, ψ, γ are defined as

$$A \equiv 4F^4 + 6F^2 r_1 + 26\,r_1^2\,, \qquad B \equiv F^4 + 39F^2 r_1 - 24\,r_1^2\,, \qquad C \equiv (4F^4 + 3F^2 r_1 + 5\,r_1^2)/(F^2 + r_1)\,,$$

$$\xi \equiv |\,\widetilde{x} - x\,|/r_1\,, \qquad \psi \equiv -(\widetilde{z}+z)/(r_1 + |\,\widetilde{x} - x\,|)\,, \qquad \gamma \equiv -(\widetilde{z}+z)/\sqrt{(\widetilde{y}-y)^2 + (\widetilde{z}+z)^2}\,.$$

The analytical approximation (6) to the local flow component G^L in (3) is considerably simpler than the exact integral representation (4) and the alternative approximations, based on table interpolations or polynomial expansions, previously given in the literature [18-20]. In particular,

the approximation (6) is valid in the entire flow region $0 \le r_1 \le \infty$. The local flow component in the gradient $\widetilde{\nabla} G$ of G is evaluated via analytical differentiation of (6). The expressions for $\widetilde{\nabla} G$ are given in [4,5] for the Green functions of thin-ship theory and the theory of flow due to a free-surface pressure patch, and in [8] for the general case of flow about an arbitrary ship hull.

The function L in expression (4) for the local flow component G^L in the Green function G is depicted in Fig.6 in the three particular cases $a = 0$ (left), $b = 0$ (center) or $c = 0$ (right), i.e. for $\widetilde{x} - x = 0$, $\widetilde{y} - y = 0$ or $\widetilde{z} + z = 0$. The function L is evaluated using the (exact) integral representation (4) or the simple analytical approximation (6) in this figure. This comparison shows that the approximation (6) is not highly accurate. However, it is asymptotically correct in both the near-field limit $r_1 \to 0$ and the far-field limit $r_1 \to \infty$. This property, important because the two limits yield major contributions, may be a primary reason for the fact that the calculations reported in [8,4,5] show that the simple analytical approximations to the local flow component (and their gradients) given in these three studies yield flow velocities in close agreement with results of calculations based on exact integral representations. Thus, the classical Green functions for steady ship waves have been greatly simplified, and a major stumbling block for the practical use of the Green function method has been removed.

II – 2 Practical evaluation of 3D flows due to source distributions

Another well-known basic difficulty associated with the practical use of the Green function method is that the flow velocity is defined by distributions of singularities (sources and dipoles) on a ship hull surface and around the mean ship waterline that require numerical evaluation of singular functions (the Green function and its gradient). However, this second stumbling block can also be removed, using a straightforward regularization approach [8]. This regularization approach is now briefly summarized.

[8] considers the basic task of evaluating the nondimensional flow velocity $\widetilde{\mathbf{u}} \equiv \widetilde{\mathbf{U}}/V_s$ due to a distribution of sources on a given (mean wetted) ship hull surface H. This flow velocity is defined as

$$\widetilde{\mathbf{u}}(\widetilde{\mathbf{x}}) \equiv \int_H da(\mathbf{x}) \widetilde{\nabla} G(\widetilde{\mathbf{x}}, \mathbf{x})\, \sigma(\mathbf{x})\,. \tag{7}$$

Here, $da(\mathbf{x})$ stands for the differential element of area of the surface H at a point $\mathbf{x}$ of H, and $\sigma(\mathbf{x})$ is the source density at $\mathbf{x}$. The usual Neumann-Kelvin theory of wavemaking also requires evaluation of the velocity due to a distribution of sources around the mean ship waterline, i.e. the intersection curve between the ship mean wetted hull surface H and the mean free-surface plane $z = 0$. This basic task is also considered in [8].

The regularization method expounded in [8] is explained here by only considering the fundamental free-space singularity $1/r$ in (3). Thus, we consider the flow velocity $\widetilde{\mathbf{u}}_r$ and the related 'regularized' velocity component $\widetilde{\mathbf{u}}_r^{reg}$ that correspond to the source distribution (7) with G taken as $4\pi G = -1/r$, i.e.

$$4\pi\, \widetilde{\mathbf{u}}_r(\widetilde{\mathbf{x}}) = \int_H da(\mathbf{x})\, \frac{\widetilde{\mathbf{x}} - \mathbf{x}}{r^3}\, \sigma(\mathbf{x}) \qquad 4\pi\, \widetilde{\mathbf{u}}_r^{reg}(\widetilde{\mathbf{x}}) = \int_H da(\mathbf{x})\, \frac{(\widetilde{\mathbf{x}} - \mathbf{x})\, \sigma(\mathbf{x})}{r^3 + \delta^6/(\delta^3 + r^3)}\,. \tag{8}$$

Here, δ stands for a small positive real number. Thus, the velocity component $\widetilde{\mathbf{u}}_r$ is expressed as the sum of a 'regularized' velocity $\widetilde{\mathbf{u}}_r^{reg}$ and the 'singular' velocity $\widetilde{\mathbf{u}}_r^S \equiv \widetilde{\mathbf{u}}_r - \widetilde{\mathbf{u}}_r^{reg}$ that accounts for the difference between the singular integrand $(\widetilde{\mathbf{x}} - \mathbf{x})/r^3$ and the corresponding 'regularized' integrand for the velocities $\widetilde{\mathbf{u}}_r$ and $\widetilde{\mathbf{u}}_r^{reg}$. Expressions (8) readily yield

$$4\pi\, \widetilde{\mathbf{u}}_r^S(\widetilde{\mathbf{x}}) \equiv \int_H da(\mathbf{x}) \left(\frac{\widetilde{\mathbf{x}} - \mathbf{x}}{r^3} - \frac{\widetilde{\mathbf{x}} - \mathbf{x}}{r^3 + \delta^6/(\delta^3 + r^3)} \right) \sigma(\mathbf{x}) = \delta^6 \int_H da(\mathbf{x})\, \frac{(\widetilde{\mathbf{x}} - \mathbf{x})\, \sigma(\mathbf{x})}{r^3 (\delta^6 + \delta^3 r^3 + r^6)}\,.$$

A straightforward analysis yields

$$2\, \widetilde{\mathbf{u}}_r^S(\widetilde{\mathbf{x}} + \nu\, \delta\, \widetilde{\mathbf{n}}) \approx \widetilde{\sigma}(\widetilde{\mathbf{x}})\, \Phi(\nu)\, \widetilde{\mathbf{n}}(\widetilde{\mathbf{x}}) \quad \text{for } \delta \ll 1\,.$$

Here, $0 \le \nu$ and the unit vector $\widetilde{\mathbf{n}} \equiv \widetilde{\mathbf{n}}(\widetilde{\mathbf{x}})$ is normal to the hull surface H and points into the fluid. Furthermore, the function $\Phi(\nu)$ is defined as

$$\Phi(\nu) \equiv \frac{1}{2}\int_0^\infty \frac{dt}{T^3(1+\nu^3 T^3+\nu^6 T^6)} \approx \frac{1-\mu\,(3.63-8.61\,\mu+11.18\,\mu^2-5.87\,\mu^3)/(1+\nu^3)}{1+1.65\,\nu+7\,\nu^6}$$

with $T \equiv \sqrt{1+t}$ and $\mu \equiv \nu^3/(1+\nu^3)$. We then have $\Phi \to 1$ and $\widetilde{\mathbf{u}}_r^S = \widetilde{\sigma}\,\widetilde{\mathbf{n}}/2$ as $\nu \to 0$. This expression shows that the velocity component $\widetilde{\mathbf{u}}_r^S$ at a point $\widetilde{\mathbf{x}}$ of a ship hull surface H is normal to H and equal to half the source density $\widetilde{\sigma}$ at $\widetilde{\mathbf{x}}$, in agreement with a classical result of potential-flow theory. The function $\Phi(\nu)$ vanishes rapidly as ν increases. Indeed, we have $\Phi \sim 1/(7\nu^6)$ as $\nu \to \infty$ and $\Phi < 0.1\%$ for ν greater than approximately 2.3.

Thus, at a flow field point $\widetilde{\mathbf{x}}$ located at a ship hull surface H, the flow velocity $\widetilde{\mathbf{u}}(\widetilde{\mathbf{x}})$ associated with the source distribution (7) on a ship hull surface H, or a similar distribution of sources around a ship waterline, and the Green function G given by (3) and (6) is expressed in [8] as

$$\widetilde{\mathbf{u}}(\widetilde{\mathbf{x}}) = \widetilde{\mathbf{u}}_W(\widetilde{\mathbf{x}}) + \widetilde{\mathbf{u}}_L^{reg}(\widetilde{\mathbf{x}}) + \widetilde{\sigma}(\widetilde{\mathbf{x}})\,\widetilde{\mathbf{n}}(\widetilde{\mathbf{x}})/2\,.$$

This flow representation expresses the flow velocity $\widetilde{\mathbf{u}}$ due to a surface (or line) distribution of sources, with density σ, on a ship hull surface (or waterline) as the sum of a wave component $\widetilde{\mathbf{u}}_W$, a 'regularized' local flow component $\widetilde{\mathbf{u}}_L^{reg}$, and a component $\widetilde{\sigma}(\widetilde{\mathbf{x}})\,\widetilde{\mathbf{n}}(\widetilde{\mathbf{x}})/2$ that accounts for the contribution of the singularity in the Green function (3) and is defined explicitly in terms of the source density σ and the unit vector $\mathbf{n}$ to the hull surface H. The wave component $\widetilde{\mathbf{u}}_W$ is associated with the Fourier integral in expression (3) for the Green function and is defined in a straightforward way using a Fourier-Kochin representation; i.e. $\widetilde{\mathbf{u}}_W$ is defined by a Fourier integral that involves a wave-spectrum function given by a surface (or line) distribution of elementary waves $e^{\,(1+t^2)\,z/F^2 - i\sqrt{1+t^2}\,(x+t\,y)/F^2}$ on the ship hull surface H (or waterline). Thus, the wave-spectrum function is given by a surface (or line) integral with integrand that only involves *continuous* ordinary functions (exp, cos, sin) of *real* arguments. Likewise, the regular local flow component $\widetilde{\mathbf{u}}_L^{reg}$ is given by a surface (or line) integral with integrand that only involves *continuous* ordinary (algebraic) functions of *real* arguments.

The flow representation given in [8] and briefly summarized here is then considerably simpler than the classical mathematical representations, which involve the exponential integral function $E(\zeta)$ of a complex argument ζ or a related special function, previously used in the literature. The surface (or line) integrals that define the wave-spectrum function in the Fourier-Kochin representation of the wave component $\widetilde{\mathbf{u}}_W$ and the local flow component $\widetilde{\mathbf{u}}_L^{reg}$ can readily be integrated analytically (for the wave-spectrum function) or via ordinary Gaussian quadrature rules (for the local flow component $-1/r + G^L$ in the expression for G), as shown in [8] for a piecewise linear distribution of sources over flat triangular hull panels or straight waterline segments. The method is then particularly simple and well suited for practical calculations.

CONCLUSION AND ONGOING WORK

As already noted in the introduction, the analytical relations for ship bow waves and the flow-calculation method summarized here are directed toward routine applications at early ship design stages, including concept and preliminary design, and hull-form optimization [21-25]. Our ongoing joint research work considers three main tasks : (a) extend the analytical bow wave profile given in [6] for a (four-parameter) family of fine nonbulbous ship bows to a more general (seven-parameter) family of bulbous bows, (b) apply the practical flow-calculation method given in [8] to investigate four alternative potential flow models based on the Neumann-Kelvin theory and variations of that classical theory, and (c) consider hull-form optimization that seeks to develop ship forms with reduced drag and motions [25].

[1] Noblesse F., Delhommeau G., Guilbaud M., Yang C. (2008) The Rise of Water at a Ship Stem, *J. Ship Research*, **52** :89-101

[2] Noblesse F., Delhommeau G., Guilbaud M., Hendrix D., Yang C. (2008) Simple analytical relations for ship bow waves, *J. Fluid Mechanics*, **600** : 105-132

[3] Delhommeau G., Guilbaud M., David L., Yang C., Noblesse F. (2009) Boundary between unsteady and overturning bow wave regimes, *J. Fluid Mechanics*, **620** :167-175

[4] Noblesse F., Delhommeau G., Kim H.Y., Yang C. (2009) Thin-ship theory and influence of rake and flare, *J. Engineering Mathematics*, **64** :49-80

[5] Noblesse F., Delhommeau G., Yang C. (2009) Practical evaluation of steady flow due to a free-surface pressure patch, *J. Ship Research*, **53** :137-150

[6] Noblesse F., Delhommeau G., Yang C., Kim H.Y., Queutey P. (2011) Analytical bow waves for fine ship bows with rake and flare, *J. Ship Research*, in press (publication scheduled for March 2011)

[7] Noblesse F., Delhommeau G., Queutey P., Yang C. (submitted) A simple approximate theory of overturning ship bow waves

[8] Noblesse F., Delhommeau G., Huang F., Yang C. (submitted) Flow due to a distribution of sources on a steadily-advancing ship hull

[9] Noblesse F., Hendrix D., Faul L., Slutsky J. (2006) Simple analytical expressions for the height, location, and steepness of a ship bow wave, *J. Ship Research*, **50** :360-370

[10] Queutey P., Visonneau M. (2007) An Interface Capturing Method for Free-Surface Hydrodynamic Flows. *Computers & Fluids*. **36** :1481-1510

[11] Löhner R., Yang C., Onate E., Idelssohn S. (1999) An Unstructured Grid-based, Parallel Free Surface Solver, *Applied Numerical Mathematics*, **31** :271-293

[12] Yang C., Löhner R. (2002) Calculation of Ship Sinkage and Trim Using a Finite Element Method and Unstructured Grids, *International Journal on Computational Fluid Dynamics*, **16** :217-227

[13] Noblesse F., Hendrix D.M., Kahn L. (1991) Nonlinear local analysis of steady flow about a ship, *J. Ship Research*, **35** :288-94

[14] Noblesse F. (1981) Alternative integral representations for the Green function of the theory of ship wave resistance, *J. Eng Mathematics*, **15** :241-65

[15] Bessho M. (1964) On the fundamental function in the theory of the wavemaking resistance of ships, *Memoirs Defense Academy*, Japan **4** :99-119

[16] Noblesse F. (1975) The near-field disturbance in the centerplane Havelock source potential, *1st Il Conf. Numerical Ship Hydrodynamics*, Washington DC, 481-501

[17] Noblesse F. (1978) On the fundamental function in the theory of steady motion of ships, *J. Ship Research*, **22** :212-215

[18] Newman J.N. (1987) Evaluation of the wave-resistance Green function : Part 1 - the double integral, *J. Ship Research*, **31** :79-90

[19] Telste J.G., Noblesse F. (1989) The nonoscillatory near-field term in the Green function for steady flow about a ship, *17th Symp. Naval Hydrodynamics*, The Hague, Netherlands, 39-52

[20] Ponizy B., Noblesse F., Ba M., Guilbaud M. (1994) Numerical evaluation of free-surface Green functions, *J. Ship Research*, **38** :193-202

[21] Percival S., Hendrix D., Noblesse F. (2001) Hydrodynamic optimization of ship hull forms, Applied Ocean Research, **23** :337-355

[22] Yang C., Soto O., Löhner R., Noblesse F. (2002) Hydrodynamic Optimization of a Trimaran, Ship Technology Research, **49** :70-92

[23] Kim H.Y., Yang C., Löhner R., Noblesse F. (2008) A practical hydrodynamic optimization tool for the design of a monohull ship, *Il Conf. Soc. Offshore & Polar Eng. (ISOPE-08)*, Vancouver, Canada

[24] Yang C., Kim H.Y., Löhner R., Noblesse F. (2008) Practical hydrodynamic optimization of ship hull forms, *Grand Challenges in Modeling & Simulation* (GCMS-08), Edinburgh, UK.

[25] Kim H.Y., Yang C., Noblesse F. (2010) Hull form optimization for reduced resistance and improved seakeeping via practical design-oriented CFD tools, *Grand Challenges in Modeling & Simulation* (GCMS-10), Ottawa, Canada.